Applied Energy 111 (2013) 669–680

Contents lists available at SciVerse ScienceDirect

Applied Energy

journal homepage: www.elsevier.com/locate/apenergy

Performance analysis of a rotary active magnetic refrigerator

J.A. Lozano [a,b], K. Engelbrecht [a,*], C.R.H. Bahl [a], K.K. Nielsen [a], D. Eriksen [a], U.L. Olsen [a], J.R. Barbosa Jr. [b], A. Smith [a], A.T. Prata [b], N. Pryds [a]

[a] Department of Energy Conversion and Storage, Technical University of Denmark, Frederiksborgvej 399, DK-4000 Roskilde, Denmark
[b] POLO Research Laboratories for Emerging Technologies in Cooling and Thermophysics, Department of Mechanical Engineering, Federal University of Santa Catarina, Florianópolis, SC 88040-900, Brazil

HIGHLIGHTS

- Experimental results of a novel rotary active magnetic refrigerator are obtained.
- Experiments are compared to predictions from a 1D numerical AMR model.
- Performance is evaluated considering parasitic losses for a range of conditions.
- A cooling power of 200 W is produced at a span of 16.8 K with a COP of 0.69.
- The attained overall second-law efficiency is around 5%.

ARTICLE INFO

Article history:
Received 6 February 2013
Received in revised form 29 April 2013
Accepted 14 May 2013
Available online 12 June 2013

Keywords:
Magnetic refrigeration
Regenerator
Coefficient of performance
Performance analysis
Efficiency

ABSTRACT

Performance results for a novel rotary active magnetic regenerator (AMR) and detailed numerical model of it are presented. The experimental device consists of 24 regenerators packed with gadolinium (Gd) spheres rotating inside a four-pole permanent magnet with magnetic field of 1.24 T. A parametric study of the temperature span, cooling power, coefficient of performance (COP) and efficiency of the system was carried out over a range of different hot reservoir temperatures, volumetric flow rates and cooling powers. Detailed modeling of the AMR using a 1D model was performed and compared with the experimental results. An overall mapping of the thermal losses of the system was performed, and good agreement between the experimental and numerical results was found when parasitic heat losses were subtracted from the modeling results. The performance of the system was evaluated via the COP, the exergetic-equivalent cooling power (Ex_Q), and the overall second law efficiency, η_{2nd}. Losses mapping indicated that friction and thermal leakage to the ambient are the most important contributors to the reduction of the system performance. Based on modeling results, improvements on the flow distributor design and reduction of the cold end thermal parasitic losses are expected to enhance the efficiency of the system. For an operating frequency of 1.5 Hz, a volumetric flow rate of 400 L/h, a hot reservoir temperature of 297.7 K, and thermal loads of 200 and 400 W, the obtained temperature spans, ΔT_S, were 16.8 K and 7.1 K, which correspond to COPs of 0.69 and 1.51, respectively. The maximum overall second-law efficiency was 5.6% for a ΔT_S of 12.9 K at 500 L/h and 400 W.

1. Introduction

An active magnetic regenerator (AMR) refrigerator is an alternative cooling technology that uses a solid refrigerant that has no ozone depleting potential and no direct global warming potential. Instead the technology relies on the magnetocaloric effect, a coupling between the temperature and magnetic field of magnetic materials. Since the magnetization/demagnetization of a magnetocaloric material (MCM) can be reversible, it may be possible to build highly efficient cooling devices around the effect for a diverse number of applications including chip and sensor cooling [1] and low-cost magnetic energy conversion devices [2].

A room temperature regenerative magnetic refrigerator was first demonstrated by Brown [3]. In 1982 the active magnetic regenerator (AMR) concept was introduced, in which the regeneration was achieved by the active material itself [4]. Since then, many new devices have been reported [5], with modern AMRs generally using permanent magnets and regenerators made of packed spheres [6,7], packed particles [8] or parallel plates [9,10] of MCM. A comprehensive overview of the material and the regenerator technology was recently given in Ref. [11]. The AMR cycle uses a heat transfer fluid to transport the heat generated from magnetizing and demagnetizing the MCM to the hot and cold reservoirs. The

* Corresponding author. Tel.: +45 46775649.
E-mail address: kuen@dtu.dk (K. Engelbrecht).

0306-2619/$ - see front matter © 2013 Elsevier Ltd. All rights reserved.
http://dx.doi.org/10.1016/j.apenergy.2013.05.039

Nomenclature

Roman

A_c	cross-sectional area of regenerator, m^2
A_{HT}	total surface area for heat transfer, m^2
B	internal magnetic field, T
c	specific heat capacity, J/(kg K)
d_h	hydraulic diameter, m
Ex_Q	exergetic-equivalent cooling power, W
f_f	friction factor, –
f	frequency of operation, Hz
h	convection coefficient, W/(m^2 K)
k_{disp}	thermal conductivity of the fluid due to axial dispersion, W/(m K)
k_{eff}	effective conductivity, W/(m K)
m	mass, kg
$\dot{m}_f$	mass flow rate of fluid, kg/s
p	pressure, bar
$\dot{Q}$	parasitic loss, W
$\dot{Q}_C$	cooling capacity, W
$\mathcal{R}$	thermal resistance, K/W
Δs_{mag}	magnetic entropy change, J/kg K
T	temperature, K
t	time, s
ΔT_{ad}	adiabatic temperature change, K
ΔT_C	temperature difference at the cold heat exchanger, K
ΔT_H	temperature difference at the hot heat exchanger, K
ΔT_S	temperature span, K
T_C	cold reservoir temperature, K
T_H	hot reservoir temperature, K
T_R	room temperature, K
$\dot{V}$	volumetric flow rate, L/h

Greek symbols

ϵ	porosity, –
η	efficiency, –
ϕ	utilization factor, –
ρ	density, kg/m^3

Subscripts

2nd	second-law
AMR	AMR cycle
comp	component
cond	conduction
conv	convection
cy	cycle
e	external
f	fluid
fl	flow distributors
i	internal
id	ideal cycle
in	inlet of the pump
mag	magnetic
M	electric motor
max	maximum
ME	mechanical and electrical
nl	no load
no-fl	without flow distributors
out	outlet of the pump
OP	overall pumping
P	pumping
rad	radiation
s	solid regenerator material
visc	viscous

Abbreviations

AMR	active magnetic regenerator
CFD	computational fluid dynamics
COP	coefficient of performance
DTU	Technical University of Denmark
Gd	gadolinium
MCM	magnetocaloric material

AMR cycle has four basic processes: magnetization, the cold-to-hot blow, demagnetization, and the hot-to-cold blow. During magnetization, the temperature of the MCM increases, then fluid is pumped from the cold reservoir to the hot reservoir in order to reject the magnetic work to ambient. The regenerator is then demagnetized, causing a decrease in temperature and a cooling load is accepted from the cooled space by pumping fluid from the hot reservoir across the regenerator and into the cold reservoir. The system performance is mostly a function of the MCM, heat transfer characteristics in the regenerator, and cycle parameters such as frequency and fluid flow rate.

Rotary AMRs, where the magnetic field in the regenerators is varied by rotating the regenerator relative to the magnet, have been shown to operate effectively at higher cycle frequencies. Devices with stationary magnets and rotating regenerators have been demonstrated by Ref. [6,12], while systems with stationary regenerators and rotating magnets have been demonstrated by Ref. [7,13–15]. Several AMR devices have been reported recently using Gd regenerators, which is the benchmark MCM for use in AMR devices. A magnetic refrigerator using stationary regenerator beds and a rotating permanent magnet was shown to produce a maximum cooling power of 844 W at zero temperature span and 400 W at a temperature span, ΔT_S, of 8.1 K using a 0.89-kg Gd regenerator [15]. This device operated continuously with a maximum reported operating frequency of 4.7 Hz, and an exergetic equivalent cooling power of 14 W was obtained. Efficiency was not reported. A rotary magnet device using a fluid displacer to distribute the fluid flow was reported to operate at a no-load temperature span of 29 K. This device produced a cooling power of 50 W at a ΔT_S of 10 K, using a 0.11-kg Gd regenerator at a maximum operating frequency of 4 Hz [16]. A maximum COP of 1.6, which included all motor inefficiencies and drive loss, was calculated for a cooling capacity of 50 W at a ΔT_S of 2.5 K and a frequency of 1.4 Hz. The COP could be increased to 2.2 if the motor inefficiency were removed [16].

The machine evaluated in this paper was described in detail in Refs. [17–20] together with some experimental results. It consists of a novel concentric magnet assembly design [21] with a 24-bed regenerator rotating continuously in the magnet gap. Fluid flow is provided by a continuously operating gear pump and flow distributor system. The flow distributors are designed such that a minimum of eight regenerator beds are open to flow at any given time to minimize fluctuations in flow to the regenerator. This device demonstrated a maximum cooling power of 1010 W at a ΔT_S of 0.3 K and a maximum no-load ΔT_S of 25.4 K and that it absorbs a cooling power, $\dot{Q}_C$, of 100 W at a ΔT_S of 21 K [18]. A maximum operating frequency of 10 Hz was experimentally proved at a ΔT_S of 12.1 K and 200 W [20].

This paper presents experimental data, numerical results obtained using a 1D model of the AMR [22] and, for the first time, a detailed assessment of the system efficiency over a range of operating conditions. The power consumption associated with several components have been measured, and methods for improving the system performance and increasing its efficiency are suggested.

A detailed thermal loss analysis of several system components was carried out, which was applied *a posteriori* to improve agreement between model and experiment. The performance of the system was evaluated in terms of COP, Ex_Q, and η_{2nd}.

2. Experimental work

The experiments were carried out on a rotary AMR device at the Technical University of Denmark (DTU). The AMR itself consists of 24 Gd-sphere packed regenerators which are rotating inside a four-pole static permanent magnet assembly. Table 1 presents the specifications of the AMR device. A more detailed description of the experimental device can be found in Ref. [18]. The regenerator beds, fabricated in nylon, of 100 mm length were packed with Gd spheres sieved to diameters between 0.25 and 0.8 mm. The permanent magnet generates a maximum magnetic flux density of 1.24 T in the four high field regions and approximately 0 T in the four low field regions [23]. The heat transfer fluid is a mixture of 20% automotive antifreeze (ethylene glycol) and 80% water by volume. The antifreeze includes corrosion inhibitors that protect the Gd regenerator in addition to reducing the freezing temperature of the fluid. Thermal load is applied to the system at the cold end by an electric resistance heater. The experiments presented in this paper were performed with an operational frequency of 1.5 Hz and the ambient temperature was kept around 295 K. The hot reservoir temperature is set by a chiller that communicates with the AMR via a brazed plate heat exchanger. The temperature of the fluid is measured by four type E thermocouples at the hot in, hot out, cold in and cold out ports of the regenerator, respectively. These thermocouples are located directly upstream or downstream of the flow distributor, depending on flow direction. The locations of the thermocouples are approximately 200 mm from the edge of the permanent magnet and are not affected by the magnetic field (Fig. 1). The volumetric flow rate is measured at the hot and cold ends after the thermocouples by a Burket Type 8081 fluid flow meter. The volumetric flow rate is controlled by a manual valve that allows bypassing the fluid across a constant flow rate pump. The cooling power to the device is the measured electrical power supplied to the resistance heater mounted in the cold reservoir (Fig. 1). Power consumption of the motor is measured by an Elnet-Pico power multimeter at the electrical plug of the frequency converter. The fluid flow distributor uses a type of face seal that allows some internal leakage in the distributor. The leakage causes fluid to bypass the regenerator directly on the hot end of the regenerator and to bypass the heater section on the cold end of the regenerator. Further details about the design, operation and experimental results can be found in Refs. [17,18,20]. The uncertainty in measured temperature span is difficult to determine because it depends on many parameters in addition to the measurement devices. Because the flow distributors use a sliding face seal, friction will slowly wear the sealing faces and change the flow conditions with time. Room temperature and air flow patterns will influence parasitic losses and change performance. The plastics used in the construction slowly absorb water and their dimensions can change due to relaxation of their molecular structure. These factors all influence the uncertainty of the experimental results and an in depth study of uncertainty as a function of hours of operation and changing ambient conditions is outside the scope of this work. The uncertainty in the measured temperature span is therefore estimated to be approximately 1 K.

Table 1
Specifications of the rotary AMR.

Property	Value	Units
Magnetic poles	4	–
Magnetic field	1.24	T
Number of regenerators	24	–
Regenerator length	100	mm
Regenerator width	12.5	mm
Regenerator height	18.6	mm
Magnetocaloric material	Commercial Gd spheres	–
Sphere diameter	0.25–0.8	mm
Regenerator volume	23.3	cm^3
Regenerator mass	0.118	kg
Total regenerator mass	2.8	kg
Operating frequency	0.25–10	Hz
Volumetric flow rate	50–600	L/h
Utilization factor	0.01–3.40	–

The temperature span is defined as the temperature difference between the time-averaged temperatures exiting the regenerator at the hot and cold ends. In this study, cooling capacities of 200 and 400 W were applied to the system while varying the hot reservoir temperature and volumetric flow rate. The tests to determine the temperature span dependence on the hot reservoir temperature were performed at the 400-L/h volumetric flow rate (measured at the cold end). Alternatively, the tests to determine the temperature span as a function of the volumetric flow rate were carried out at a hot reservoir temperature of 297.7 K.

The cooling capacity associated with the regenerator is a function of the solid regenerator mass, m_s and the specific heat capacity, c_s. These parameters are often combined with the mass of the heat transfer fluid, m_f, that flows through the regenerator in one blow period, and the fluid specific heat, c_f, to define the utilization factor, ϕ, which represents the ratio of the fluid and regenerator thermal capacities as follows [24],

$$\phi = \frac{m_f c_f}{m_s c_s} \tag{1}$$

The specific heat used in Eq. (1) is the average specific heat at zero field over the operating temperature span of the regenerator.

3. Modeling

3.1. Numerical simulation

Several numerical models of AMR systems have been reported in the literature [25]. Among those, one-dimensional models are characterized for been practical and flexible for performance analysis of AMRs [26]. In this paper, the experiments presented were modeled using a 1D porous AMR model from Ref. [22,27] to quantify thermal losses and seek ways to improve performance. The model solves the 1D regenerator equations shown in Eqs. (2) and (3) using an implicit solver. The governing equation for the heat transfer fluid, which includes dissipation due to pressure drop, is:

$$\dot{m}_f c_f \frac{\partial T_f}{\partial x} + hA_{HT}(T_f - T_s) + \rho_f A_c \epsilon c_f \frac{\partial T_f}{\partial t} - k_{disp} A_c \frac{\partial^2 T_f}{\partial x^2} = \left| \frac{f_f \dot{m}_f^3}{2\rho_f^2 A_c^2 d_h} \right| \tag{2}$$

where T is temperature, ρ is density, c is specific heat, h is the heat transfer coefficient, A_{HT} is the area for heat transfer, ϵ is the porosity, $\dot{m}_f$ is the fluid mass flow rate, k_{disp} is the thermal conductivity of the fluid due to axial dispersion, f_f is the friction factor and A_C is the cross-sectional area. The terms represent (in order from left to right) the enthalpy change of the fluid associated with the flow, heat transfer from the fluid to the solid, energy storage, energy transfer due to axial dispersion associated with mixing of the fluid, and viscous dissipation due to pumping losses. The governing equation for the solid regenerator material is:

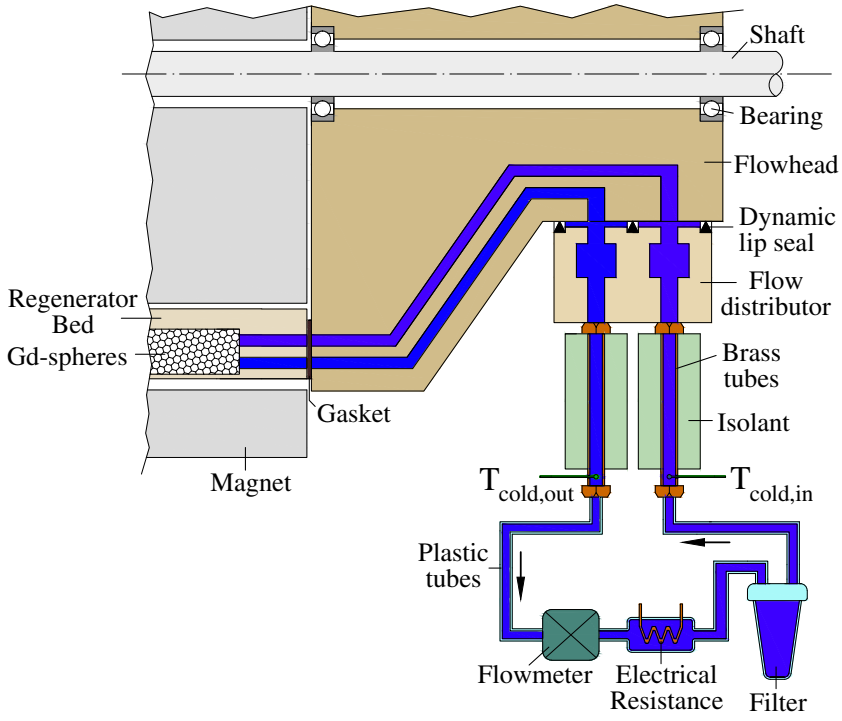

Fig. 1. Schematic representation of the cold end of the experimental device.

$$hA_{HT}(T_f - T_s) + k_{eff}\frac{\partial^2 T_s}{\partial x^2} = (1-\epsilon)\rho_s T_s\left(\frac{\partial s_s}{\partial B}\right)_T \frac{\partial B}{\partial t} + (1-\epsilon)\rho_s c_{B,s}\frac{\partial T_s}{\partial t} \quad (3)$$

where B is the internal magnetic field of the solid regenerator that is corrected for the demagnetizing field and k_{eff} is the effective thermal conductivity of the fluid and solid matrix. The terms represent heat transfer from the fluid to the regenerator, non-dispersive or static axial conduction (through the composite of the regenerator and fluid), magnetic work transfer, and energy storage. A detailed description of the model is given in Ref. [27]. For the modeling done here, a MCM property function of the specific commercial grade Gd used in the machine was developed using in-house measurements of the zero-field specific heat [28] and magnetization at several magnetic fields and temperatures of the Gd spheres [20]. Some of the properties of the commercial Gd spheres implemented in the numerical model are presented in Table 2. The overall demagnetization factor calculated for the packed sphere regenerator beds was 0.365 based on Ref. [29,30]. The magnetic field profile as a function of the angular position in the gap was measured using a Hall probe inside the actual magnet. The temporal mass flow profile in each regenerator was calculated using the geometry of the flow distributors and flow inlets to the regenerator beds. However, the actual mass flow profile cannot be experimentally measured and may be slightly different for each regenerator bed due to variations in sphere packing and the flow path to each regenerator bed. Also, the small fluid leakage that occurs in both the hot and cold end flow distributors was ignored in the numerical model. The steady state temperature profile is determined by starting from a given temperature profile and stepping the governing equations forward until the temperature at every point in the regenerator is the same at the beginning and end of the cycle within a numerical tolerance.

Table 2
Properties of the commercial Gd spheres implemented in the numerical model.

Property	Value	Units
Sphere diameter	0.6	mm
Regenerator porosity	0.36	–
Density	7901	kg/m^3
Thermal conductivity	11	W/(m K)
Maximum Δs_{mag} (at 288 K and 1 T)	3.2	J/(kg K)
Maximum ΔT_{ad} (at 290 K and 1 T)	3.1	K
Regenerator demagnetization factor	0.365	–
Room temperature	295	K

The numerical model [27] considers only a porous regenerator subjected to a specified fluid flow in the presence of a varying magnetic field. It does not account for phenomena such as thermal and mechanical interaction with the polymer regenerator housing, heat losses from the regenerator to the ambient, or losses in the external piping. In this study, losses to the ambient are post-calculated and subtracted from the cooling power predicted by the model. As will be seen, these losses to the ambient have a significant impact on the predicted performance and should be accounted for in a more detailed model of the AMR.

3.2. Parasitic losses analysis

The entire system experiences thermal leakage either to the ambient in the form of heat losses or from the ambient in the form of an added cooling load, depending on the temperature of the specific part of the machine. Since the total area of tubing and flow distribution components is relatively large, it is important to predict the magnitude of the losses and to examine their impact on the system performance. As mentioned above, the parasitic losses are post-calculated and subtracted from the predicted cooling power obtained by the 1D AMR numerical simulation. This section discusses how losses from the various components are calculated. All losses are estimated based on correlations for simplified geometries available in the literature.

Using the electrical circuit analogy, a thermal resistance, $\mathcal{R}$, was calculated for each heat transport mechanism associated with each major component in the system:

$$\mathcal{R}_{comp} = \mathcal{R}_{conv,i} + \mathcal{R}_{cond} + \frac{\mathcal{R}_{conv,e}\mathcal{R}_{rad}}{\mathcal{R}_{conv,e} + \mathcal{R}_{rad}} \quad (4)$$

where $\mathcal{R}_{cond}$, $\mathcal{R}_{conv,i}$, $\mathcal{R}_{conv,e}$ and $\mathcal{R}_{rad}$ are the calculated thermal resistances associated with the heat transport to the ambient due to conduction through the walls, internal and external convection and external radiation, respectively. It should be noted that the external convection and external radiation act in parallel with respect to the surface to ambient temperature difference. The thermal parasitic loss of each component, $\dot{Q}_{comp}$, is calculated as,

$$\dot{Q}_{comp} = \frac{T_R - T_C}{\mathcal{R}_{comp}} \tag{5}$$

As shown in Fig. 1, the cold end is composed mainly of a flowhead, a flow distributor, connecting tubes, and a filter. The experimental temperatures are measured downstream of the flow distributors, while the numerical model considers only the fluid temperature entering and exiting the regenerator bed ends. For modeling purposes, it was assumed that the fluid at the cold end has a uniform temperature throughout at the cold end. For the calculation of thermal parasitic losses, a room temperature T_R = 295 K was assumed, which is a close approximation to the average temperature for all experiments.

Brass tubes are used downstream of the flow distributor and plastic tubing is used upstream of it. In the experiments presented here thermal insulation was applied only to the brass tubes, while the remaining components at the hot and cold ends were not insulated. The thermal resistance of the tubes and filter at the cold end are calculated assuming that they behave as cylinders under free convection. The flowhead (fabricated in nylon) consists of 24 pairs of channels that allow the fluid flow from the beds into the flow distributor. Due to the relative complexity of the geometry, a 2D numerical simulation was carried out in COMSOL [31] to determine the heat transfer rate from the ambient to the cold fluid associated with a pair of channels, as shown in Fig. 1. It is assumed that each regenerator bed has the same inlet and outlet temperature and the difference between them is 1 K, which is a typical value for regenerators investigated here. Since the inner diameter of the flowhead is quite large and not subjected to the ambient conditions, it is assumed adiabatic.

Several parasitic losses studies in AMR devices have shown that the main thermal losses are due to mechanical friction in the seals and bearings, which gives rise to inconsistency in experimental repeatability and represents a decrease in performance [32–34].

In the present device, there is heating in the flow distributor due to friction between the dynamic lip seals and the inner surface of the flow distributor with the outer surface of the flowhead. In order to calculate the heat generated at the seals, measurements of the motor power were performed with and without the flow distributor, for different frequencies at room temperature. The power consumption due to friction in the distributor was calculated as the difference between the motor power with and without it.

In the numerical model the walls of the regenerator beds are considered adiabatic, but in reality there will be heat transfer to the ambient through the regenerator walls along the entire length of the regenerator. In this study, a calculation procedure to estimate the heat flow through the upper wall to or from the ambient is proposed. Since the regenerator beds are rotating in the gap of the concentric magnets, forced convection can be assumed to take place in the gaps over the regenerator beds. The distance between the beds and the magnets is much smaller than the diameter of the magnet, so a parallel-plate geometry, for which the laminar flow Nusselt number is 7.54, is assumed. It is important to note that there is a temperature gradient inside the beds in the axial direction. Therefore, thermal losses in the regenerator beds were calculated by the integral of the thermal gradient along the regenerator bed. Because of its relatively high thermal conductivity, the temperature of the magnet is assumed equal to that of the ambient. Heat transfer was only assumed to occur through the upper wall of the regenerator beds, while the remainder of their surface area was assumed adiabatic because the nylon wall thickness is larger in those places and the inner diameter is not exposed directly to ambient.

Other parasitic losses were disregarded, such as those due to eddy currents in the Gd beds that are constantly magnetized and demagnetized. However, the total power due to eddy currents in the spheres is expected to be small in comparison with the cooling capacity of the AMR device because of the small particle size.

4. Performance metrics

The thermodynamic performance of the rotary magnetic refrigerator was quantified in terms of three different parameters: the coefficient of performance, COP, the exergetic-equivalent cooling power, Ex_Q, and the overall second law efficiency, η_{2nd}.

4.1. COP definitions

The COP is defined as the ratio between the cooling capacity and the power consumption of the system. According to Ref. [35], the system COP can be calculated as the following product,

$$COP = COP_{id} \cdot \eta_e \cdot \eta_{cy} \cdot \eta_P \cdot \eta_{ME} \tag{6}$$

where the factors in Eq. (6) will be detailed below. By definition, the actual COP can be written as,

$$COP = \frac{\dot{Q}_C}{\dot{W}_P + \dot{W}_M} \tag{7}$$

where $\dot{W}_P$ and $\dot{W}_M$ are the electrical powers required to drive the fluid pump and the motor that rotates the regenerator assembly, respectively.

The COP of an ideal, i.e., totally reversible, refrigerator device, COP_{id}, is defined as:

$$COP_{id} = \frac{\dot{Q}_C}{\dot{W}_{id}} \tag{8}$$

where $\dot{W}_{id}$ is the power consumed by an ideal cooling cycle operating within the temperature limits of the hot and cold environments, T_H and T_C, respectively. In the present system, it corresponds to an ideal magnetic power since there is no fluid friction in the entire (ideal) refrigerator.

In terms of the hot and cold environment temperatures, the COP of the ideal (Carnot) device is given by:

$$COP_{id} = \frac{T_C}{T_H - T_C} \tag{9}$$

In order to account for external irreversibilities associated with hot and cold heat exchangers, the external thermodynamic efficiency can be defined as:

$$\eta_e = \frac{COP_{id,e}}{COP_{id}} \tag{10}$$

where $COP_{id,e}$ is the Carnot COP calculated using the temperatures of the heat exchangers as follows:

$$COP_{id,e} = \frac{T_C - \Delta T_C}{(T_H + \Delta T_H) - (T_C - \Delta T_C)} \tag{11}$$

where ΔT_H and ΔT_C correspond to the finite temperature differences at the hot and cold heat exchangers, respectively, due to the finite area for heat transfer. Thus, when $\Delta T_{C,H} \to 0$ the system is externally reversible as $\eta_e \to 1$. For a specific cooling capacity, $\eta_{id,e}$ can be seen as the ratio of magnetic powers needed to magnetize and demagnetize the material between the limits of the

environment temperatures and the heat exchangers temperatures as follows,

$$\eta_e = \frac{\dot{W}_{id}}{\dot{W}_{mag}} \tag{12}$$

As mentioned above, in the device evaluated in this paper, T_H is set by a chiller connected to a heat exchanger. On the cold side, the cooling load is provided by an electric heater.

The internal thermodynamic losses associated with the cooling cycle are calculated based on the viscous power of the working fluid, $\dot{W}_{visc}$ through the regenerator beds and the magnetic power, $\dot{W}_{mag}$. Therefore, the cycle efficiency, η_{cy}, can be defined as:

$$\eta_{cy} = \frac{\dot{W}_{mag}}{\dot{W}_{mag} + \dot{W}_{visc}} \tag{13}$$

where

$$\dot{W}_{visc} = \dot{V}_f(p_{out} - p_{in}) \tag{14}$$

In Eq. (14), p_{out} and p_{in} are the measured fluid pressures at the outlet and inlet of the pump.

Based on the definitions in Eqs. (9)–(14), the cycle COP, which accounts for internal and external thermal losses in the cooling cycle is given by,

$$COP_{cy} = COP_{id} \cdot \eta_e \cdot \eta_{cy} = \frac{\dot{Q}_C}{\dot{W}_{visc} + \dot{W}_{mag}} \tag{15}$$

The mechanical losses associated with the pumping of the fluid, i.e., losses at the pump, are calculated based on the fluid pumping power, $\dot{W}_P$, and $\dot{W}_{mag}$. So a pumping efficiency, η_P, can be defined as:

$$\eta_P = \frac{\dot{W}_{mag} + \dot{W}_{visc}}{\dot{W}_{mag} + \dot{W}_P} \tag{16}$$

where

$$\dot{W}_P = \frac{\dot{W}_{visc}}{\eta_{OP}} \tag{17}$$

and η_{OP} is the overall pump efficiency, assumed equal to 0.7.

The power, $\dot{W}_M$, needed to overcome the magnetic torque and rotate the flow distributors is provided by an electric motor. Thus, the combined mechanical and electrical efficiency is given by:

$$\eta_{ME} = \frac{\dot{W}_P + \dot{W}_{mag}}{\dot{W}_P + \dot{W}_M} \tag{18}$$

where $\dot{W}_M$ is made up of three parts, namely, the magnetic power, $\dot{W}_{mag}$, the power needed to rotate the flow distributors over the flowhead (which gives rise to the oscillating flow in the regenerator beds) and overcome friction between their sliding surfaces, $\dot{W}_{fl}$, and the power associated with other mechanical losses (i.e., those which remain when the flow distributors are not in place and when the system is not loaded with magnetic material in the regenerators - e.g., gear coupling, belt drive, frequency inverter, etc.), $\dot{W}_{nl}$. Thus,

$$\dot{W}_M = \frac{\dot{W}_{mag} + \dot{W}_{fl}}{\eta_M} + \dot{W}_{nl} \tag{19}$$

where η_M is the electric motor efficiency, assumed to be 0.8.

Experimentally the motor power, $\dot{W}_M$, is measured as the plug power consumed by the frequency inverter. The motor power is broken into three parts, as shown in Eq. (19) which allows the definition of two additional (hypothetical) performance factors. The COP_{AMR} is the COP of the actual AMR excluding mechanical and electrical losses external to the regenerator, but intrinsic to the actual driving system. Thus:

$$COP_{AMR} = \frac{\dot{Q}_C}{\frac{\dot{W}_{visc}}{\eta_{OP}} + \left(\frac{\dot{W}_{mag} + \dot{W}_{fl}}{\eta_M}\right)} \tag{20}$$

In contrast, the COP_{no-fl} is defined so that it takes into account all mechanical and electrical losses in the system, but *excludes* the losses associated with friction in the flow distribution system.

$$COP_{no-fl} = \frac{\dot{Q}_C}{\dot{W}_P + \dot{W}_M - \dot{W}_{fl}} \tag{21}$$

While COP_{AMR} excludes the losses that take place outside the regenerator, COP_{no-fl} accounts for the losses associated with friction in the flow distribution system which, as shown above, have been estimated experimentally in the present paper.

4.2. Exergetic-equivalent cooling capacity

Even though the COP is widely used to compare refrigeration systems, it is of limited significance when the temperature span is not specified. The exergetic-equivalent cooling power [36], given by,

$$Ex_Q = \dot{Q}_C\left(\frac{T_H}{T_C} - 1\right) \tag{22}$$

is an important parameter to quantify the performance of an AMR as it is directly proportional to the temperature span and cooling power, indicating that a high performance refrigerator is one in which a wide thermal load is transferred to the hot thermal reservoir over a high temperature span. Note that Ex_Q is not equal to the actual cooling power of the machine but it is the exergy associated with the cold reservoir.

4.3. Second-law efficiency

The second law (or exergy) efficiency, η_{2nd}, has been used as a performance metric to compare different cooling technologies [37]. It is defined as the ratio of the power consumed by the actual device to that of a reversible system within the same temperature span associated with the hot and cold environments. In terms of the COPs, it is given by,

$$\eta_{2nd} = \frac{COP}{COP_{id}} \tag{23}$$

where COP and COP_{id} are calculated from Eqs. (7) and (9), respectively.

Experiments on a 450-liter top-mount household vapor compression refrigerator at ambient temperatures ranging from 298.4 to 316.3 K indicated a second-law efficiency of ~21% [35].

The second-law efficiency associated with the thermodynamic performance of the cooling cycle only, $\eta_{2nd,cy}$, takes into account the irreversibilities due to the viscous losses and magnetization and demagnetization process in the AMR. Thus,

$$\eta_{2nd,cy} = \frac{COP_{cy}}{COP_{id}} \tag{24}$$

allows for a comparison of the present system with different cooling technologies using the same thermodynamic baseline. Therefore, it helps to provide indications of where system improvements can be made.

5. Results and discussions

5.1. Parasitic losses

The motor power was measured at different operating frequencies and load conditions as follows: (i) with the regenerators and

both flow distributors installed, $\dot{W}_M$; (ii) with the regenerators, but without the flow distributors (see Fig. 1), $\dot{W}_{no-fl}$; (iii) only with the frequency inverter that controls the motor, $\dot{W}_{nl}$. The friction loss associated with the flow distribution system is computed as follows:

$$\frac{\dot{W}_{fl}}{\eta_M} = \dot{W}_M - \frac{\dot{W}_{mag}}{\eta_M} - \dot{W}_{nl} = \dot{W}_M - \dot{W}_{no-fl} \quad (25)$$

where the two terms on the right of the second equality are determined experimentally. It is important to point out that $\dot{W}_M$ was measured for each experiment presented in this work as a function of the temperature span, while $\dot{W}_{no-fl}$ and $\dot{W}_{nl}$ were measured at an average temperature of 295 K at zero temperature span as it is impossible to maintain a temperature gradient across the regenerator without the flow distributors. As can be seen from Fig. 2, $\dot{W}_{fl}/\eta_M$ varies approximately linearly with frequency. The friction heat generated in the flow distributor is rejected to the working fluid, to the flow distributor housing and to the ambient. A full thermal analysis of the flow distributors is outside the scope of this paper, so it is assumed that half the friction heat is transferred to the fluid. The heat load due to friction in the flow distributor which is transferred to the fluid at the cold end is calculated by $\dot{Q}_{fl} = (13.2f - 2.5)$, where f is the frequency. This equation corresponds to a linear fit of the experimental test results obtained at different frequencies. Since the experiments presented here were all carried out at 1.5 Hz, then the heat transferred to the fluid is assumed to be $\dot{Q}_{fl}(f = 1.5Hz) \simeq 17.3$ W. The assumption that half the heat is transferred to the fluid adds to the uncertainty of the thermal losses, which are discussed below.

The magnetic work, $\dot{W}_{mag}$, which includes magnetic parasitic losses, such as eddy currents, is estimated from the experimental results as follows:

$$\frac{\dot{W}_{mag}}{\eta_M} = \dot{W}_{no-fl} - \dot{W}_{nl} \quad (26)$$

It should be noted that the value of $\dot{W}_{mag}$ estimated with this experimental procedure is not the actual magnetic work on the regenerator when either a temperature gradient in the matrix or a net cooling power are produced. This is because $\dot{W}_{no-fl}$ and $\dot{W}_{nl}$ were measured at a constant temperature in the regenerator (zero temperature span), thus taking into account only the effect of frequency. However, the error associated with this approximation is expected to be small since $\dot{W}_{mag}/\eta_M$ is much smaller than $\dot{W}_M$ (see Fig. 2).

In Fig. 2, $\dot{W}_{mag}/\eta_M$ is seen to be much smaller than the friction power loss in the flow distributor. For comparison purposes, $\dot{W}_P$ at 1.5 Hz, calculated through Eq. (17), for $\Delta T_S = 10$ K and $\dot{V}_f = 400$ L/h, is about 42 W.

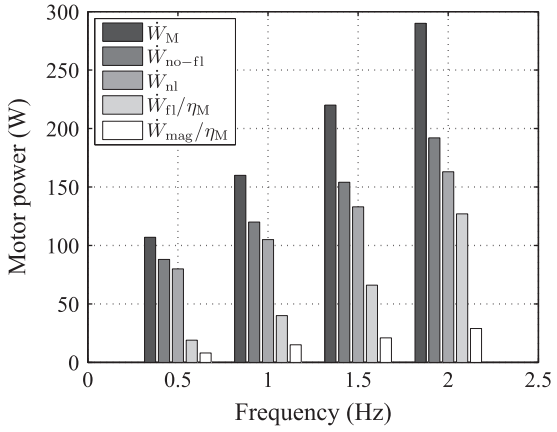

Fig. 2. Breakdown of the motor power for different operating frequencies. Measurements were performed at 295 K.

The calculated thermal resistances for each component are summarized on Table 3. From the CFD modeling of the heat transfer in the flowhead, it was found that most of the heat is lost from the flow channel nearest the outer wall through the outer wall, to the ambient rather than conducted to the adjacent fluid stream. Since the flowhead is rotating with the regenerator and has a relatively large diameter, the heat transfer through its outer surface was modeled as forced convection over a flat plate. With this boundary condition the COMSOL simulation of the heat transfer in the fluid channels yielded an overall thermal resistance of 1.05 K/W in the flowhead.

The estimated parasitic losses associated with each component as a function of T_C is shown in Fig. 3 for $T_R = 295$ K, $T_H = 300$ K and $f = 1.5$ Hz. The total heat loss, $\dot{Q}_{total}$, is calculated as the sum of all parasitic losses including $\dot{Q}_{fl}$, which is considered independent of T_C. As expected, thermal parasitic losses increase as T_C decreases and ΔT_S increases. When T_C is above room temperature, there are negative heat losses as the working fluid rejects heat to the ambient, which artificially increases the cooling capacity. The total parasitic losses at a temperature span of 25 K are estimated to be 74 W, a significant value which must be overcome by the AMR in order to maintain the temperature span.

When operating at high frequencies, the most important contribution to the parasitic losses is the flow distributor friction, which, in principle, is only a function of frequency. This contribution can be minimized with a new hydraulic design of the flow distribution system. Additionally, in order to achieve higher temperature spans or cooling capacities, a good thermal insulation over the flowhead, tubes and filter should be employed, or these components should be redesigned to minimize the heat transfer area. The regenerator bed losses are more complicated to deal with because any increase in the wall thickness will reduce the amount of magnetized volume occupied by the regenerator. The regenerator wall also participates in the regeneration process as it is subjected to oscillating flow and temperature conditions. Improving the regenerator insulation involves a trade-off between MCM volume and parasitic losses; this study requires detailed modeling to investigate further and it is outside the scope of this paper.

Heat leaks at the hot end were also investigated. However, they are less important because the heat rejected at the hot end is not measured experimentally and is not a major performance parameter. Heat leaks from most of the hot end components can be viewed as additional heat exchanger area for heat rejection as they are at approximately the same temperature as the hot heat exchanger. The situation is also different at the hot end because the fluid is cooled by the ambient but heated by the flow distributor friction. The main concern from a modeling standpoint is that the experimental hot reservoir temperature may differ from the fluid temperature actually entering the regenerator. Because the hot reservoir temperature is measured before the fluid enters the flow distributor upstream the regenerator, there will be a difference between the measured hot reservoir temperature and that of the fluid entering the regenerator, which is the temperature used in the numerical model. An analysis of heat losses at the hot end revealed

Table 3
Thermal resistances of the components at the cold end and the regenerator beds.

Component	Thermal resistance (K/W)
Insulated brass tubes	9.21
Plastic tubes	1.84
Filter	1.66
Flowhead	1.05
Regenerator beds	0.54

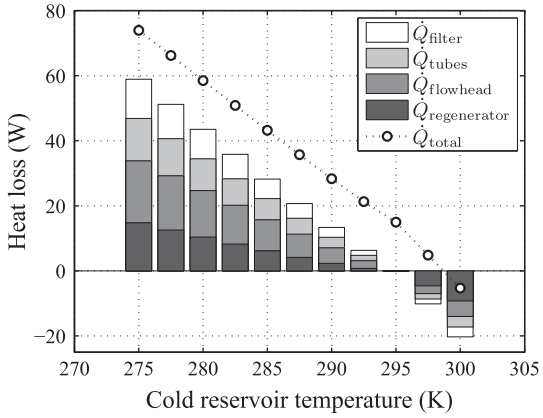

Fig. 3. Parasitic losses for the different components at different temperatures at the cold end. $\dot{Q}_{total}$ corresponds to the total parasitic losses including also $\dot{Q}_{fl} = 17.3$ W.

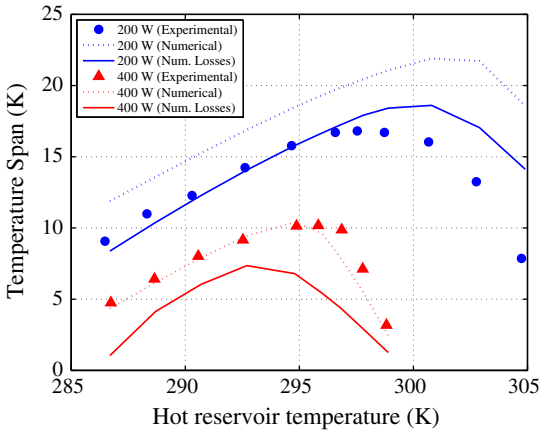

Fig. 4. Experimental data and numerical predictions of temperature span with and without the post-calculated parasitic losses for cooling loads of 200 and 400 W effect of hot reservoir temperature.

that in the worst case scenario, i.e., when the hot reservoir temperature is 290 K, a loss of approximately 20 W from the fluid in the hot reservoir would take place. For a volumetric flow rate of 200 L/h, this loss results in a reduction of 0.09 K between the measurement point and the regenerator inlet, which is within the uncertainty of the thermocouple measurements. Therefore, hot end losses are not considered further.

5.2. Experimental results

The experimental study of the system consists of evaluating the temperature span as a function of the hot reservoir temperature as well as the volumetric flow rate at different cooling loads.

5.2.1. Hot reservoir temperature dependence

The influence of the hot reservoir temperature on the temperature span for cooling loads of 200 and 400 W was determined experimentally by varying the temperature in the chiller at the hot end. The experimental data is plotted in Fig. 4 and compared with the 1D model results with and without the influence of the post-calculated parasitic losses. The experiments reported in Fig. 4 were carried out with a volumetric flow rate of 400 L/h (ϕ is approximately 0.37, depending on the operating temperature), measured at the cold end. The temperature span corresponds to the temperature difference between the temperature of the fluid exiting the hot end and the temperature of the fluid exiting the cold end of the regenerator.

In Fig. 4, the shape and peak temperature of the temperature span as a function of T_H are related to the magnetocaloric properties of the refrigerant. As explained in [38], the maximum temperature span, $\Delta T_{S,max}$, does not occur at the Curie temperature, but at a hot reservoir temperature above the Curie temperature. For cooling loads of 200 and 400 W, $\Delta T_{S,max}$ values of 16.8 K and 10.2 K were obtained for hot reservoir temperatures of T_H of 297.7 K and 296 K, respectively. The dependence of the optimum hot reservoir temperature on cooling load shown in Fig. 4 can be explained by studying the operating temperatures of the regenerator. The optimum hot reservoir temperature for a given cold reservoir temperature is one that maximizes the magnetocaloric effect over the entire regenerator, which will generally occur when the Curie temperature of the material is near the midpoint between the hot and cold reservoir temperatures. As the cooling load increases, the cold reservoir temperature increases. As the cold reservoir temperature increases, the optimum hot reservoir temperature will decrease accordingly to keep the material's Curie temperature near the midpoint between the two reservoir temperatures.

As can be seen from Fig. 4, there is good agreement between model and experiment when T_H is below 300 K for a cooling power of 200 W. For higher values of T_H, the model under predicts the experiment when thermal losses are included. However, when thermal losses are ignored, the model over predicts the cooling power as would be expected. The reason for the discrepancy is not known, but it may be caused by variation in the friction heating in the flow distributors with varying temperature. Considering results when T_H is approximately 302 K, for example, the hot flow distributor will be at a higher temperature than other experiments, but the cold flow distributor will also be at a higher temperature than the 300 K case. If thermal expansion in the flow distributors and changing properties in the radial seals causes flow distributor friction to be reduced with increasing temperature, this could explain the reason that thermal losses seem to be over predicted at higher T_H values.

Experimental results for a cooling power of 400 W differ somewhat significantly from the numerical results with post-calculated parasitic losses. Although no clear cause of the discrepancy has been identified, this may be due to a number of reasons. At a higher cooling power the device operates at a lower temperature span and a larger portion of the regenerator operates near the Curie temperature where the magnetocaloric effect is highest. Therefore the high cooling power experiments are more sensitive to material properties. Because the Gd used in the regenerator is commercial grade purchased from a commercial supplier it is possible that the average Curie temperature in the regenerator is different than small sample that was measured, causing the device to produce a higher cooling power than predicted at a certain temperature range. Another area of uncertainty is the experimental characterization of the particle size distribution, which becomes more pronounced at higher cooling power conditions. An extended discussion on this issue will be presented in Section 5.3.

5.2.2. Volumetric flow rate dependence

In the second set of experiments, the hot reservoir temperature was kept approximately at 297.7 K and the volumetric flow rate was varied. The dependence of the latter on temperature span as well as the values predicted from the numerical model including the parasitic losses are plotted in Fig. 5. The temperature span increases with increasing volumetric flow rate. Due to working pressure limitations and internal leakage in the flow distribution system, it was not possible to operate the device at flow rates above 600 L/h.

Based on results shown in Fig. 5, the temperature span is expected to continue to decrease at higher flow rates as viscous flow losses increase with the square of the flow rate for the 200 W case. A slight increase in temperature span for the 400 W case may be possible for higher flow rates, but the model predicts only a small increase temperature span at higher flow rates. As can be seen in the figure, there is good agreement between the experimental data and the model results. At lower volumetric flow rates, the numerical results under predict the performance while at higher volumetric flow rates the model overestimates the temperature span results. The highest experimental temperature spans at 200 W and 400 W were attained at 500 L/h and 600 L/h with values of 17.5 K and 13.8 K, respectively.

5.3. Inputs sensitivity

Achieving excellent agreement between model and experiment is challenging due to the level of uncertainty associated with the input parameters. In the regenerator, each bed will experience a unique flow rate due to differences in flow resistances between the beds. The parasitic losses are based on simplified correlations; however, air flow and conditions in the room where the device is placed can change from day to day and even with the time of day, so the exact parasitic losses to the ambient may be highly variable and are difficult to predict accurately. The regenerator is modeled as a monodisperse matrix, but the actual regenerators contain a distribution of sphere sizes. It is also known that there is internal leakage in the flow distributor at the hot and cold side, which results in the actual flow rate in the regenerator being different than the flow rate that goes to the heater to accept a cooling power. There are many other uncertainties such as heat transfer in the sphere bed, properties of the housing materials, etc. A thorough understanding of these effects is outside the scope of this paper and, therefore, the simplified approach is considered appropriate. To estimate the effect of these uncertainties on modeling results, a brief sensitivity study was performed and the results are summarized in Fig. 6. This figure shows two different cases; one case where the cooling capacity is 200 W and the volumetric flow rate is 400 L/h and the other where the cooling capacity is 400 W and the flow rate is 600 L/h. It can be seen that if the sphere diameters are changed within ±25% the predicted temperature span will change ±12% and ±20% at 200 and 400 W cooling loads, respectively. On a different note, if the total heat losses are increased by a factor of 1.25 the temperature span is decreased about 4%. The values in Fig. 6 will not be the same for each experimental condition, but they do give an estimate of how each uncertainty affects the results and what the modeling uncertainty is.

5.4. Performance evaluation results

The performance of the system is evaluated in terms of the COP, Ex_Q and η_{2nd}.

5.4.1. COP analysis

The different COPs proposed in this work were calculated for all the experiments using Eqs. (6)–(21), where $\dot{Q}_C$ corresponds to the thermal load applied at the cold end by the electrical resistance heater. Figs. 7 and 8 show the results of COP, COP_{no-fl} and COP_{AMR} as a function of the hot reservoir temperature and the volumetric flow rate, respectively. The temperature span for each COP value corresponds to those plotted in Figs. 4 and 5.

In Fig. 7, the (experimental) COP seems to be independent of the hot reservoir temperature, with average results for cooling powers of 200 W and 400 W of 0.71 and 1.50 and maximum COP of 0.77 at $T_H = 304.7$ K and 1.60 at $T_H = 298.8$ K, respectively. However, the COP increases at higher hot reservoir temperatures probably due to a decrease in the power of the motor since the hot and cold ends are warmer (the temperature span is lower) and the gadolinium is less ferromagnetic. On the other hand, even though ΔT_S increases with $\dot{V}_f$ (Fig. 5), the COP is inversely proportional to the volumetric flow rate, with a maximum of 1.00 at $\dot{V}_f = 200$ L/h and $\dot{Q}_C = 200$ W, and 1.62 at $\dot{V}_f = 350$ L/h and $\dot{Q}_C = 400$ W, as shown in Fig. 8.

From the results presented in Figs. 7 and 8 it can be inferred that an improvement of the performance of the system could be attained by reducing the power applied to the motor. The motor power is consumed by its internal losses, gear couplings, frequency inverter, belt drive, friction in the flow distributors and bearings and, to a lesser extent, by the magnetization and temperature change of the Gd with the fluid flow. Therefore, a hypothetical enhancement of the performance of this machine could be achieved with an improved design of the flow distributors. Assuming a new design with no friction in the flow distributors, the increase in COP can be as high as 24%, as shown in Figs. 7 and 8 for COP_{no-fl}.

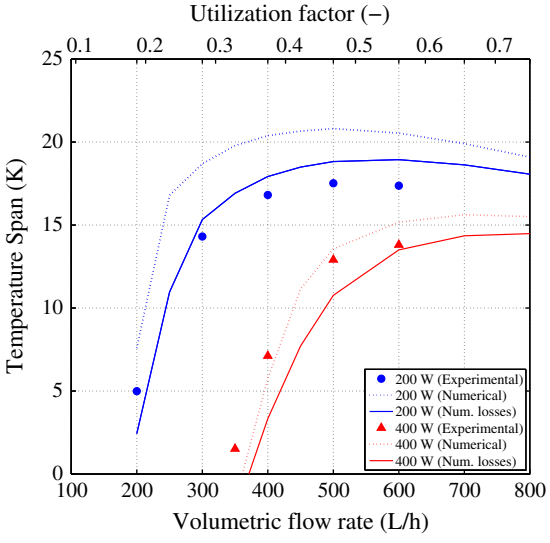

Fig. 5. Experimental data and numerical predictions of the temperature span with and without the post-calculated parasitic losses for cooling loads of 200 and 400 W effect of volumetric flow rate.

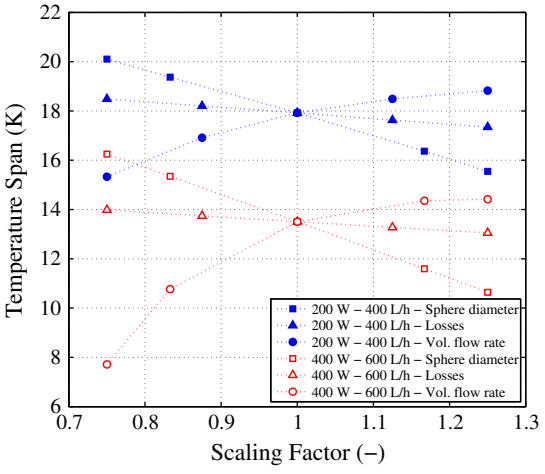

Fig. 6. Temperature span as a function of the scaling factor of the volumetric flow rate, total losses and sphere diameter for cases with volumetric flow rates of 400 L/h and 600 L/h and cooling power of 200 W and 400 W, respectively.

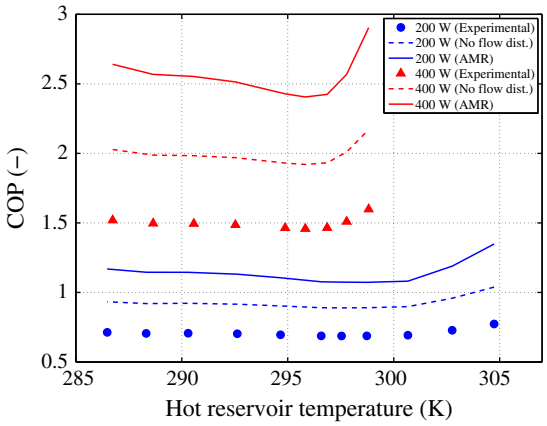

Fig. 7. Comparison of COP, COP_{no-fl} and COP_{AMR} as a function of the hot reservoir temperature for cooling loads of 200 W and 400 W.

The electrical motor is oversized in order to cover a broad range of experiments, with high torques at operating frequencies up to 10 Hz [20]. In a real application, the motor would be selected for a specific narrow range of operating conditions of the AMR. Therefore, an estimate was made for the COP of an actual AMR using an appropriate motor to overcome the magnetic torque at a frequency of 1.5 Hz. Supposing the efficiency of an appropriate motor for these conditions is included in the calculated values from Eqs. (25) and (26), an average improvement of COP_{AMR} of 48% over COP, with values of COP_{AMR} up to 3.5, can be accomplished if a high-efficiency motor is employed. In Figs. 7 and 8, COP_{AMR} is consistently higher than COP_{no-fl} because the motor losses are bigger than those in the flow distributors, as seen in Fig. 2.

A typical value of COP_{cy}, derived from the results presented in Section 5.1, for $f = 1.5$ Hz, $\dot{Q}_C = 400$ W, $T_H = 295$ K, $\Delta T_S = 10$ K and $\dot{V}_f = 400$ L/h, was calculated to be of about 8.6. It is worth mentioning that COP and COP_{id} for this case are 1.46 and 30.4, respectively, which represent a $\eta_{2nd} = 4.8\%$ and a $\eta_{2nd,cy} = 28.4\%$.

5.4.2. Exergetic-equivalent cooling capacity

The exergetic-equivalent cooling power, Ex_Q, of the system as a function of the hot reservoir temperature and volumetric flow rate is shown in Figs. 9 and 10, respectively. The trend of Ex_Q as a function of the hot reservoir temperature resembles those reported in the literature [15]. For a volumetric flow rate of 400 L/h and cooling capacities of 200 and 400 W, the maximum Ex_Q obtained was 12.0 and 14.2 W, respectively. For a fluid flow rate of 600 L/h the Ex_Q was 19.4 W.

5.4.3. Second law efficiency

Overall and cycle second-law efficiencies as a function of the hot reservoir temperature and volumetric flow rate are presented in Figs. 11 and 12, respectively.

The results for the cycle second-law efficiency, $\eta_{2nd,cy}$, somewhat mirrors the behavior of ΔT_S and Ex_Q, in the sense that it is high when ΔT_S is large. This is because the temperature span becomes small at high and low values of T_H and, in behaving as such, gives rise to high values of COP_{id} (see Eq. (9)). At intermediate values of T_H, $\eta_{2nd,cy}$ becomes high due to the more efficient conversion of magnetic work into cooling effect, which results in larger values of ΔT_S, and hence smaller values of COP_{id}.

The behavior of the overall second-law efficiency, η_{2nd}, is flatter due to the mechanical losses which are less dependent on T_H and $\dot{V}_f$ than the thermodynamic losses accounted for in $\eta_{2nd,cy}$. The cycle second-law efficiency depends mainly on the regenerator's end temperatures and at higher hot reservoir temperatures $\eta_{2nd,cy}$ strongly decreases since the cold end temperatures are higher and the temperature spans are lower. Moreover, the results in Figs. 11 and 12 help to quantify the influence of these mechanical losses as well as the maximum achievable efficiency (in comparison with a Carnot refrigerator operating within the same environment temperature span).

The maximum values of η_{2nd} and Ex_Q obtained with the present system were of the order of 5% and 15–20 W, which are somewhat modest figures in comparison with established cooling technologies. For instance, in a household refrigerator of average cooling capacity of 80 W at $T_H \sim 305$ K, η_{2nd} approaches 21% with an $Ex_Q \sim 15$ W (average ΔT_S of 47 K) [35]. The 30-W (nominal) cooling capacity Stirling, reciprocating compressor and linear compressor portable coolers investigated in [37] exhibited, at $T_H \sim 305$ K, overall second-law efficiencies of around 14%, 14% and 8%, respectively, which corresponded to Ex_Q of 4.3, 4.7 and 5.9 W. A thermoelectric cooler of similar characteristics evaluated in the same study presented an overall second-law efficiency of only 1%.

Considering the fact that magnetic cooling at room temperature is still a developing technology, improvements in mechanical design and material selection can certainly contribute to reducing the gap between actual and idealized performance (Figs. 11 and

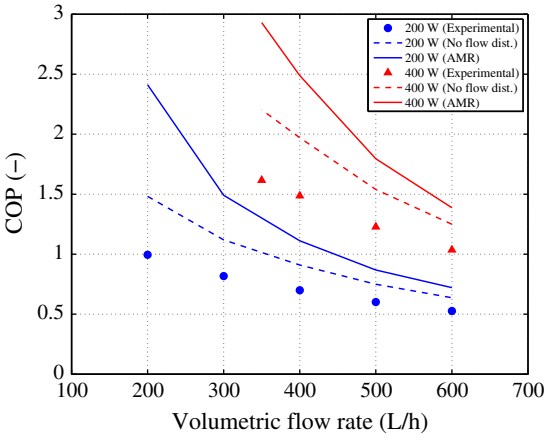

Fig. 8. Comparison of COP, COP_{no-fl} and COP_{AMR} as a function of the volumetric flow rate for cooling loads of 200 W and 400 W.

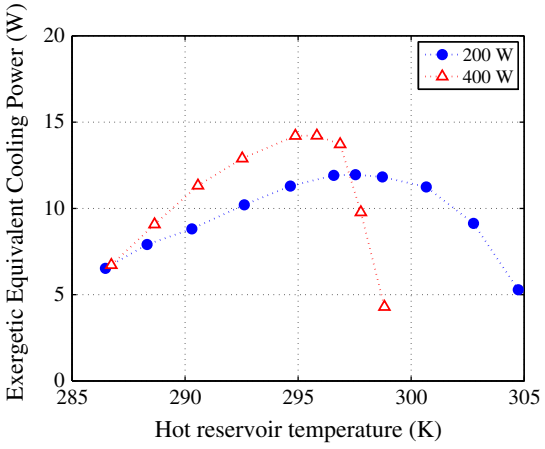

Fig. 9. Exergetic-equivalent cooling power as a function of the hot reservoir temperature for cooling powers of 200 W and 400 W.

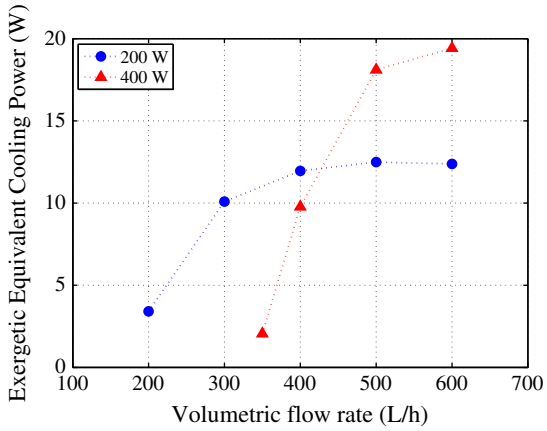

Fig. 10. Exergetic-equivalent cooling power as a function of the volumetric flow rate for cooling powers of 200 W and 400 W.

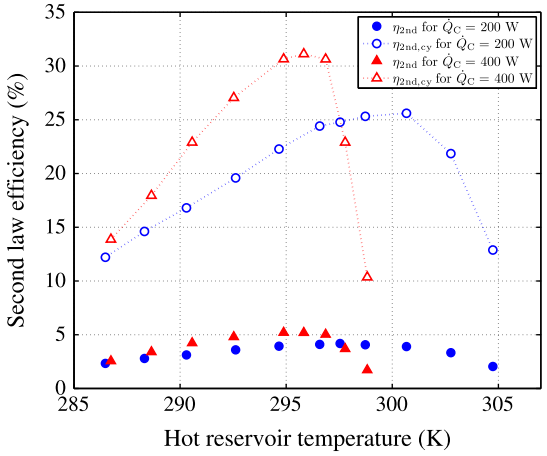

Fig. 11. Overall and cycle second-law efficiency as a function of the hot reservoir temperature for cooling loads of 200 and 400 W.

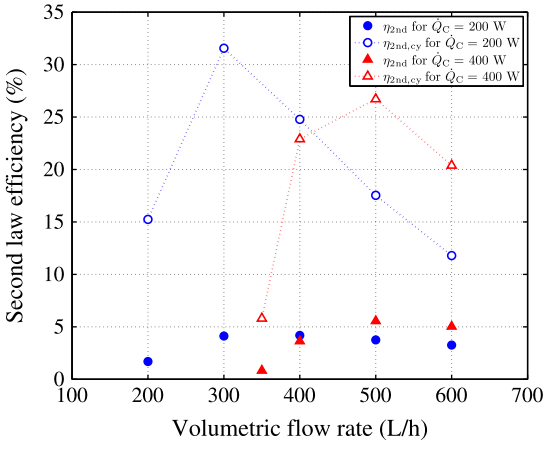

Fig. 12. Overall and cycle second-law efficiency as a function of the volumetric flow rate for cooling loads of 200 W and 400 W.

12), as well as the gap between the performance of competing technologies for certain niche applications.

A summary of the results generated in this study is presented on Table 4.

Table 4
Selected experimental results obtained at the AMR running at an operational frequency of 1.5 Hz.

T_H (K)	$\dot{V}_f$ (L/h)	ϕ (–)	ΔT_S (K)	$\dot{Q}_C$ (W)	$\dot{W}_M$ (W)	$\dot{W}_P$ (W)	COP (–)	Ex_Q (W)	η_{2nd} (%)	$\eta_{2nd,cy}$ (%)
297.7	400	0.37	16.8	200	241	45	0.70	12.0	4.2	24.8
297.7	300	0.28	14.3	200	223	22	0.82	10.1	4.1	31.6
297.7	600	0.56	13.8	400	274	112	1.04	19.4	5.0	20.4
297.7	500	0.47	12.9	400	253	73	1.23	18.1	5.6	26.7
296.0	400	0.37	10.2	400	233	41	1.46	14.2	5.2	31.1
286.9	400	0.37	4.8	400	218	45	1.52	6.7	2.6	13.9
299.0	400	0.37	3.2	400	215	35	1.60	4.3	1.7	10.4
297.7	350	0.33	1.5	400	221	26	1.62	2.1	0.8	5.8

6. Conclusions

Experimental results obtained with a novel rotary magnetic cooler prototype for a range of hot reservoir temperatures, cooling capacities and volumetric flow rates were presented. As a part of the analysis of the AMR performance, a detailed study of parasitic losses external to the regenerator beds was carried out. It was shown that flow distributor friction, heat transfer from the regenerator housing, heat losses from the connecting piping and heat losses from the cold end fluid filter contributed to reducing the performance of the AMR. When the AMR operates with a temperature span of 25 K, the losses to the ambient are estimated at approximately 74 W, which will directly reduce the power available for cooling. The efficiency of the AMR was studied for a range of operating conditions. For an operating frequency of 1.5 Hz, a volumetric flow rate of 400 L/h, and a hot reservoir temperature of 297.7 K, a cooling capacity of 200 W produced over a 16.8 K span with a COP of 0.69. For a 400-W cooling power, the temperature span was 7.1 K, with a COP of 1.51. The maximum experimentally measured COP was 1.62 when absorbing 400 W cooling power at a span of 1.5 K.

The power loss associated with various components was quantified, which made clear that efficiency can be significantly increased by reducing friction in the fluid flow distributors. Efficiency can be further increased by reducing parasitic losses, which will increase the effective cooling power of the device.

The experiments were compared to predictions from a 1D numerical AMR model for all experiments presented. When the calculated parasitic losses are included, good agreement between the model and experiment is achieved. This suggests that a simple 1D regenerator model can be used to predict a large scale AMR device with some accuracy.

The paper also presented a systematic performance evaluation of the AMR device, which incorporated the data on mechanical losses in the various components and quantified the thermodynamic and mechanical efficiencies in a second-law framework. The maximum overall second-law efficiency was around 5%, which corresponded to approximately one-sixth of the maximum second-law efficiency calculated excluding the mechanical losses. This, together with the possibility of advanced magnetocaloric materials with multiple layers can certainly make magnetic refrigeration at room-temperature more competitive at certain niche applications, as suggested by [39].

Acknowledgements

The technical support of Jørgen Geyti is greatly appreciated. The authors would like to acknowledge the support of the Programme Commission on Energy and Environment (EnMi) (Contract No. 2104-06-0032) which is part of the Danish Council for Strategic Research and CNPq (Brazil) through Grant No. 573581/2008-8

(National Institute of Science and Technology in Cooling and Thermophysics). K.K. Nielsen wishes to thank the Danish Council for Independent Research, Technology and Production Sciences (Contract No. 10-092791).

References

[1] Silva DJ, Bordalo BD, Pereira AM, Ventura J, Araujo JP. Solid state magnetic refrigerator. Appl Energy 2012;93:570–4.
[2] Vuarnoz D, Kitanovski A, Gonin C, Borgeaud Y, Delessert M, Meinen M, et al. Quantitative feasibility study of magnetocaloric energy conversion utilizing industrial waste heat. Appl Energy 2012;100:229–37.
[3] Brown GV. Magnetic heat pumping near room temperature. J Appl Phys 1976;47:3673–80.
[4] Barclay JA, Steyert WA. Active magnetic regenerator. US Patent 4,332,135; 1982.
[5] Yu B, Liu M, Egolf PW, Kitanovski A. A review of magnetic refrigerator and heat pump prototypes built before the year 2010. Int J Refrig 2010;33:1029–60.
[6] Zimm C, Boeder A, Chell J, Sternberg A, Fujita A, Fujieda S, et al. Design and performance of a permanent-magnet rotary refrigerator. Int J Refrig 2006;29:1302–6.
[7] Jacobs S, Auringer J, Boeder A, Chell J, Komorowski L, Leonard J, et al. The performance of a large-scale rotary magnetic refrigerator. In: Fifth international conference on magnetic refrigeration at room temperature; 2012.
[8] Lu DW, Xu XN, Wu HB, Jin X. A permanent magnet magneto-refrigerator study on using Gd/Gd-Si-Ge/Gd-Si-Ge-Ga alloys. In: First international conference on magnetic refrigeration at room temperature; 2005.
[9] Engelbrecht K, Bahl CRH, Nielsen KK. Experimental results for a magnetic refrigerator using three different types of magnetocaloric material regenerators. Int J Refrig 2011;30(4):1132–40.
[10] Balli M, Sari O, Mahmed C, Besson Ch, Bonhote Ph, Duc D, et al. A pre-industrial magnetic cooling system for room temperature application. Appl Energy 2012;98:556–61.
[11] Smith A, Bahl CRH, Bjørk R, Engelbrecht K, Nielsen KK, Pryds N. Materials challenges for high performance magnetocaloric refrigeration devices. Adv Energy Mater 2012;2:1288–318.
[12] Tusek J, Zupan S, Sarlah A, Prebi I, Poredos A. Development of a rotary magnetic refrigerator. Int J Refrig 2010;33:294–300.
[13] Okamura T, Yamada K, Hirano N, Nagaya S. Performance of a room-temperature rotary magnetic refrigerator. Int J Refrig 2006;29:1327–31.
[14] Vasile C, Muller C. Innovative design of a magnetocaloric system. Int J Refrig 2006;29:1318–26.
[15] Russek S, Auringer J, Boeder A, Chell J, Jacobs S, Zimm C. The performance of a rotary magnet magnetic refrigerator with layered beds. In: Fourth international conference on magnetic refrigeration at room temperature; 2010.
[16] Tura A, Rowe A. Permanent magnet magnetic refrigerator design and experimental characterization. Int J Refrig 2011;34:628–39.
[17] Bahl CRH, Engelbrecht K, Bjørk R, Eriksen D, Smith A, Nielsen KK, et al. Design concepts for a continuously rotating active magnetic regenerator. Int J Refrig 2011;34:1792–6.
[18] Engelbrecht K, Eriksen D, Bahl CRH, Bjørk R, Geyti J, Lozano JA, et al. Experimental results for a novel rotary active magnetic regenerator. Int J Refrig 2012;35:1498–505.
[19] Bahl CRH, Engelbrecht K, Eriksen D, Lozano JA, Bjørk R, Geyti J, et al. Development and experimental results from a 1 kW prototype AMR. In: Fifth international conference on magnetic refrigeration at room temperature; 2012.
[20] Lozano JA, Engelbrecht K, Bahl CRH, Nielsen KK, Barbosa Jr JR, Prata AT, et al. Experimental and numerical results of a high frequency rotating active magnetic refrigerator. In: Fifth international conference on magnetic refrigeration at room temperature; 2012.
[21] Bjørk R, Bahl CRH, Smith A, Christensen DV, Pryds N. An optimized magnet for magnetic refrigeration. J Magn Magn Mater 2010;322:3324–8.
[22] Engelbrecht K, Bahl CRH. Evaluating the effect of magnetocaloric properties on magnetic refrigeration performance. J Appl Phys 2010;108:123918.
[23] Bjørk R, Bahl CRH, Smith A, Pryds N. Improving magnet designs with high and low field regions. IEEE Trans Magn 2011;47:1687–92.
[24] Rowe A, Tura A, Dikeos J, Chahine R. Near room temperature magnetic refrigeration. In: Proceedings of the international green energy conference; 2005.
[25] Nielsen KK, Tusek J, Engelbrecht K, Schopfer S, Kitanovski A, Bahl CRH, et al. Review on numerical modeling of active magnetic regenerators for room temperature applications. Int J Refrig 2011;34:603–16.
[26] Aprea C, Maiorino A. A flexible numerical model to study an active magnetic refrigerator for near room temperature applications. Appl Energy 2010;87:2690–8.
[27] Engelbrecht K. A numerical model of an active magnetic regenerator refrigerator with experimental validation. PhD thesis, University of Wisconsin Madison; 2008.
[28] Jeppesen S, Linderoth S, Pryds N, Theil Kuhn L, Buch Jensen J. Indirect measurement of the magnetocaloric effect using a novel differential scanning calorimeter with magnetic field. Rev Sci Instrum 2008;79.
[29] Coey JMD. Magnetism and magnetic materials. Cambridge University Press; 2010.
[30] Aharoni A. Demagnetizing factors for rectangular ferromagnetic prisms. J Appl Phys 1998;83:3432–4.
[31] AB Comsol Multiphysics. Tegnergatan 23, SE-111 40 Stockholm, Sweden; 2008.
[32] Zimm C, Jastrab A, Sternberg A, Pecharsky VK, Gschneidner Jr KA, Osborne M, et al. Description and performance of a near-room temperature magnetic refrigerator. Adv Cryog Eng 1998;43:1759–66.
[33] Tura A, Roszmann J, Dikeos J, Rowe A. Cryogenic active magnetic regenerator test apparatus. Adv Cryogen Eng Trans Cryogen Eng Conf 2006;823:985–92.
[34] Arnold DS, Tura A, Rowe A. Experimental analysis of a two-material active magnetic regenerator. Int J Refrig 2011;34:178–91.
[35] Gonçalves JM, Melo C, Hermes CJL, Barbosa Jr JR. Experimental mapping of the thermodynamic losses in vapor compression refrigeration systems. J Brazilian Soc Mech Sci Eng 2011;33:159–65.
[36] Rowe A. Configuration and performance analysis of magnetic refrigerators. Int J Refrig 2011;34:168–77.
[37] Hermes CJL, Barbosa Jr JR. Thermodynamic comparison of peltier, stirling, and vapor compression portable coolers. Appl Energy 2012;91:51–8.
[38] Trevizoli PV, Barbosa Jr JR, Ferreira RTS. Experimental evaluation of a Gd-based linear reciprocating active magnetic regenerator test apparatus. Int J Refrig 2011;34:1518–26.
[39] Aprea C, Greco A, Maiorino A. A numerical analysis of an active magnetic regenerative refrigerant system with a multi-layer regenerator. Energy Convers Manage 2011;52:97–107.